# A $^{13}C$ and $^{2}H$ Nuclear Magnetic Resonance Study of Phosphatidylcholine/Cholesterol Interactions: Characterization of Liquid–Gel Phases†

T.-H. Huang,‡ C. W. B. Lee,§ S. K. Das Gupta,§ A. Blume,∥ and R. G. Griffin*,§

*Francis Bitter National Magnet Laboratory and Department of Chemistry, Massachusetts Institute of Technology, Cambridge, Massachusetts 02139, Institute of Biomedical Sciences, Academia Sinica, Taipei 11529, Taiwan, and Department of Chemistry, Universität Kaiserslautern, D-6750 Kaiserslautern, Germany*

*Received September 2, 1993*⊛

ABSTRACT: A detailed study on the structure, dynamics, and thermodynamic behavior of phosphatidylcholine/cholesterol (PC/CHOL) mixtures was undertaken using differential scanning calorimetry (DSC) and solid-state nuclear magnetic resonance (NMR) spectroscopy. DSC thermograms of mixtures of cholesterol (CHOL) with 1,2-dipalmitoyl-*sn*-phosphatidylcholine (DPPC), 1,2-distearoyl-*sn*-phosphatidylcholine (DSPC), and 1,2-diarachidoyl-*sn*-phosphatidylcholine (DAPC) showed a broadening of the first-order gel → liquid crystalline transition and a decrease in the transition enthalpy, indicating a gradual loss of cooperativity for high CHOL concentrations. DPPC and DSPC were labeled with $^{13}C$ at the carbonyl group of the *sn*-2 chain and $^{2}H$ was introduced into the middle of the *sn*-2 chain at the 6- and 12-position for DPPC and DSPC, respectively. The $^{13}C$ and $^{2}H$ NMR spectra of each labeled lipid were studied as a function of temperature and CHOL concentration. The residual quadrupole splitting in the $^{2}H$ NMR spectra, $\Delta\nu_{Q\perp}$, was analyzed as a function of temperature and composition. For CHOL concentrations less than 30 mol %, a precipitous change in $\Delta\nu_{Q\perp}$ occurs near the chain melting temperature of the phospholipid. Further increases in CHOL concentration broaden the transition and shift the midpoint to higher temperature, indicating the presence of a new phase at higher CHOL contents. Moreover, at a given temperature, $\Delta\nu_{Q\perp}$ increases with increasing cholesterol content, which indicates a more ordered structure. The $^{13}C$ NMR spectra in the gel state consisted of a superposition of two components which can be attributed to both gel-like and fluid phospholipid domains in the bilayer. This two-component spectrum can be simulated quantitatively with a two-parameter chemical exchange model, which permits the fraction of each form and the exchange rate to be determined as a function of temperature and composition. At high CHOL contents the line width of the fluid component broadens, suggesting an increase in the exchange rate between the domains. These results were interpreted in terms of a temperature composition diagram with one region $L_{\beta'}$, two regions $LG_I$ and $LG_{II}$, and one liquid crystalline region $L_\alpha$, with LG denoting "liquid–gel" type phases. Liquid–gel phases correspond to phases with increased order in the hydrocarbon chains (in comparison to that of the pure PC bilayer in the $L_\alpha$ phase) combined with fast limit axial diffusion that averages the $^{13}C$ NMR spectrum to a "fluidlike" line. These phases are similar to those found in phosphatidylethanolamine/cholesterol (PE/CHOL) mixtures [Blume, A., & Griffin, R. G. (1981) *Biochemistry 24*, 6230] and are in agreement with the results of Vist and Davis [(1990) *Biochemistry 29*, 451].

Cholesterol (CHOL)[1] can be found in many biological membranes at very high concentrations, up to 50 mol % in the case of the human erythrocyte. Although its function in the membrane is not well understood, it is postulated to maintain membrane integrity under a variety of physiological conditions by mediating membrane fluidity. Consequently, its interaction with other membrane components, such as phospholipids, is of interest. Since biological membranes are heterogeneous entities, consisting of different lipid species together with a variety of proteins, the use of a model membrane system consiting of a single phospholipid species can provide insight into the physical effects of CHOL.

Numerous studies on the physical properties of CHOL/lipid bilayers have been published [for reviews, see Demel and De Kruijff (1976), Huang (1977), Melchior (1982), Yeagle (1985), and Cullis et al. (1985)]. Early investigations on mixtures of PC and CHOL revealed that CHOL condenses fluid phospholipid monolayers while fluidizing solid ones (Shah & Shulman, 1967). Subsequent DSC studies have shown that CHOL broadens the gel-to-liquid crystalline phase transition, as well as decreasing the calorimetrically observed transition enthalpy (Ladbrooke et al., 1968; Mabrey et al., 1978; Estep et al., 1978). Thus, CHOL was postulated to order the liquid crystalline phase and disorder the gel phase. As discussed below, this view is only partially correct.

On the molecular level, the details of the PC/CHOL interaction have been examined by a variety of techniques including EPR (Shimshick & McConnell, 1973a,b; Recktenwald & McConnell, 1981), fluorescence polarization (Rubenstein et al., 1967; Calhoun & Shipley, 1979; Rand et al., 1980), electron diffraction (Hui & He, 1983), neutron scattering (Mortensen et al., 1988), freeze–fracture electron microscopy (Copeland & McConnell, 1980; Lentz et al., 1980), and NMR (Gally et al., 1976; Haberkorn et al., 1977; Brown

† This research was supported by the National Institutes of Health (GM-25505 and RR-00995). C.W.B.L. was supported in part by a fellowship from the National Sciences and Engineering Research Council of Canada. A.B. was supported by grants from the Deutsche Forschungsgemeinschaft and Fonds der Chemischen Industrie.

‡ Academia Sinica.

§ MIT.

∥ Universität Kaiserslautern.

⊛ Abstract published in *Advance ACS Abstracts*, November 15, 1993.

[1] Abbreviations: CHOL, cholesterol; DAPC, 1,2-diarachidoyl-*sn*-phosphatidylcholine; DPPC, 1,2-dipalmitoyl-*sn*-phosphatidylcholine; DSPC, 1,2-distearoyl-*sn*-phosphatidylcholine; PC, phosphatidylcholine; PE, phosphatidylethanolamine; DSC, differential scanning calorimetry; EPR, electron paramagnetic resonance; NMR, nuclear magnetic resonance; $T_m$, lipid chain melting temperature.

0006-2960/93/0432-13277$04.00/0 

& Seelig, 1978; Wittebort et al., 1982; Vist & Davis, 1990). These studies demonstrated the condensing effect of CHOL in the $L_\alpha$ phase. In particular, for $T > T_m$ of the pure lipid, addition of CHOL leads to an incease in the orientational order of the phospholipid hydrocarbon chains. In addition, CHOL enhances rotational diffusion of the lipids in the bilayer. Several of these reports have suggested the formation of specific phospholipid–cholesterol complexes [for a summary, see Lentz et al. (1980)], but a number of stoichiometries for these complexes have been proposed, as diverse as 7.5, 20, 22, 25, 30, 33, 47, and 50 mol % CHOL/mol of lipid. Other studies revealed no complex formation (Stockton & Smith, 1976; Jacobs & Oldfield, 1979), while yet others proposed multiple complexes (Lentz et al., 1980).

Partial PC/CHOL phase diagrams have been constructed (Shimshick & McConnell, 1973a,b; Gershfeld, 1978; Lentz et al., 1980; Rand et al., 1980; Recktenwald & McConnell, 1981; Blume & Griffin, 1982; Mortensen et al., 1988), and different experimental techniques have led to different proposed phases. However, recent investigations (Vist & Davis, 1990; Ipsen et al., 1988) have converged on a more consistent interpretation of the PC/CHOL system.

In this study, we have employed a combination of calorimetry and $^2H$ and $^{13}C$ solid-state NMR to examine the phase equilibria and dynamical behavior of the PC bilayer in the presence of varying concentrations of CHOL. The DSC experiments constitute a systematic study of phospholipids with differing hydrocarbon chain lengths and are in general agreement with previously published results. $^2H$ NMR spectra were useful in characterizing the $L_\alpha$ phase but exhibited complex behavior in the gel phases. In contrast, the $^{13}C$ NMR results are particularly informative of gel phase behavior. Previously published results (Wittebort et al., 1981, 1982; Blume et al., 1982; Blume & Griffin, 1982) have shown that, in going from the gel-to-liquid crystalline state, the $^{13}C$ spectrum of the *sn*-2 carbonyl position in glycerophospholipids transforms from an axially symmetric powder spectrum to an isotropic line. This spectral change is due to rotational diffusion and a conformational change at the glycerol backbone region of the lipid. Furthermore, the appearance of the isotropic line, which is diagnostic for fluid lipids, can be induced by the addition of CHOL.

The model system used in this study consist of binary mixtures of DPPC/CHOL and DSPC/CHOL, two phospholipids with hydrocarbon chains of differing lengths. It is necessary to study both species because one of the primary physical effects used to detect phase changes is the *sn*-2 $^{13}C{=}O$ spectrum, which transforms to a narrow line in the $L_\alpha$ phase. However, in the $P_{\beta'}$ phase, the line shape consists of a sharp line superimposed upon a powder spectrum similar to that induced by CHOL in the gel phase, an effect which could complicate the interpretation of the spectra. In contrast to DPPC, DSPC has a narrow $P_{\beta'}$ region and the sharp line is due almost exclusively to the addition of CHOL. The amount of CHOL was varied from 0 to 50 mol % and a wide temperature range was sampled. $^2H$ NMR experiments were performed with specifically deuterated PC, either 2-[6,6-$^2H_2$]-DPPC or 2-[12,12-$^2H_2$]DSPC. $^{13}C$ NMR experiments utilized *sn*-2 carbonyl-labeled PC, 2-[1-$^{13}C$]DPPC or 2-[1-$^{13}C$]DSPC. The experimentally derived temperature/composition diagram is compared with results from earlier studies as well as with theoretical descriptions of the PC/CHOL bilayer.

## EXPERIMENTAL PROCEDURES

*Materials.* Cholesterol, DPPC, DSPC, and DAPC were obtained from Sigma Chemical Co. (St. Louis, MO, or Deisenhofen, Germany). [1-$^{13}C$]Palmitic and stearic acids were purchased from Cambridge Isotope Labs (Woburn, MA). $^2H$-Labeled fatty acids were synthesized according to previously published methods (Das Gupta et al., 1982). $^{13}C$- and $^2H$-labeled phosphatidylcholines were synthesized by acylation of the corresponding lysophosphatidylcholine with the fatty acid anhydride using *N*,*N*-dimethyl-4-aminopyridine as a catalyst (Gupta et al., 1977). Purity was routinely checked with TLC on silica gel plates both before and after NMR measurements.

*DSC Sample Preparation.* Phospholipid suspensions with and without CHOL were prepared by mixing appropriate amounts of chloroform stock solution of CHOL with the respective phospholipid. Chloroform was removed rapidly under a stream of $N_2$ gas at 50 °C. Residual chloroform was removed under high vacuum for at least 12 h. After addition of doubly glass-distilled water, the samples were first vortexed at temperatures above the phase transition of the lipid and then sonicated for 2–5 min using an MSE 100W ultrasonic distintegrator. After further equilibration at temperatures above $T_m$ for 1 h, the suspensions were placed in the calorimetric cell.

*NMR Sample Preparation.* Samples for the NMR experiments consisted of approximately 50 mg of PC together with the appropriate amount of CHOL, which were codissolved in chloroform and evaporated under a stream of dry $N_2$ gas. Residual solvent traces were removed under a vacuum of $10^{-2}$ Torr. The samples were dispersed in an equal weight of $H_2O$ ($^2H$-depleted $H_2O$ for $^2H$-labeled samples) and sealed in 7-mm glass tubes.

*Calorimetry.* DSC measurements were performed as previously described (Blume, 1980, 1983) using a Privalov DASM-1M DSC calorimeter. For the detection of the broad transitions in lipid/cholesterol mixtures the establishment of a highly reproducible base line is important. The base line obtained with pure buffer or water was subtracted from the curves obtained with the lipid dispersions prior to data evaluation. Lipid concentrations varied between 1 and 8 mg/mL, depending on cholesterol content. The lipid concentrations were determined by phosphorus analysis using a modified procedure after Hague and Bright (1941). A scan rate of 1 °C/min was used for all experiments. Data evaluation and simulation were performed using the ORIGIN DSC software supplied by MicroCal, Inc. (Amherst, MA). For the simulation of overlapping DSC peaks a two-state model is used, with the calorimetric $\Delta H$, the van't Hoff $\Delta H$, and the transition temperature as variable parameters for each peak. Nonlinear least-squares fitting is accomplished using the Levenberg–Marquardt algorithm.

*NMR Spectroscopy.* $^{13}C$ and $^2H$ NMR spectra were obtained on a home-built spectrometer operating at 73.9 MHz for $^{13}C$, 45.1 MHz for $^2H$, and 296 MHz for $^1H$. $^2H$ NMR spectra were obtained with a quadrupole echo sequence (Davis et al., 1976) with a $\pi/2$ pulse of less than 2.0 $\mu$s. $^{13}C$ NMR spectra were obtained with either a Hahn echo or cross-polarization, with a 180° refocusing pulse to minimize base line distortion (Pines et al., 1973; Griffin, 1981). The $^{13}C$ $\pi/2$ pulse was 3 $\mu$s. Temperature control to 0.5 °C was achieved with a gas flow system described elsewhere (Wittebort et al., 1981). $^{13}C$ spectra are referenced to external tetramethylsilane (TMS).

## RESULTS

*Differential Scanning Calorimetry.* The DSC scans displayed in Figure 1 show the well-known effects of CHOL on the phase transition of phospholipid bilayers. With increasing

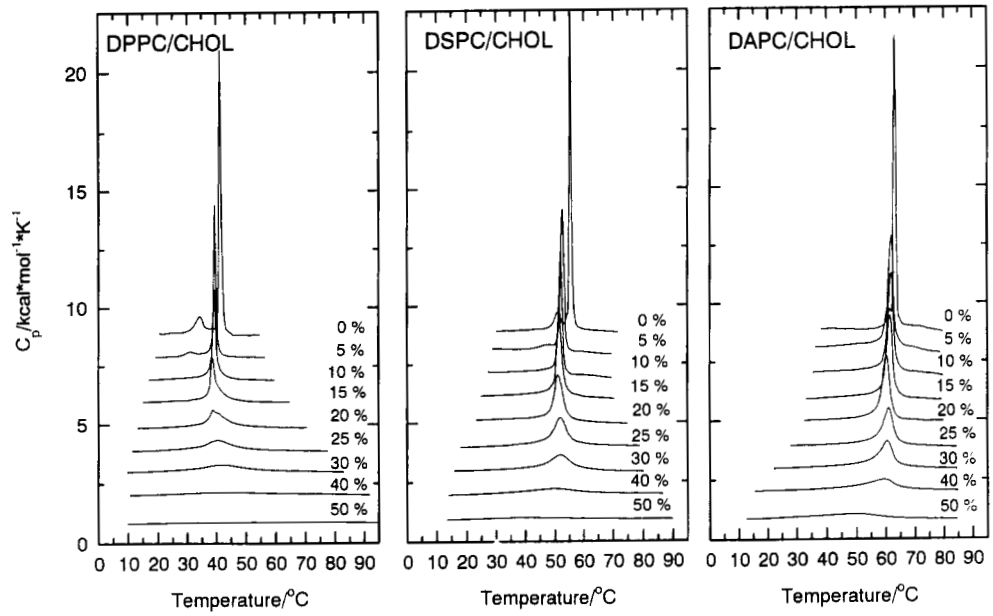


FIGURE 1: DSC thermograms of DPPC/CHOL, DSPC and DAPC/CHOL mixtures as a function of CHOL content.

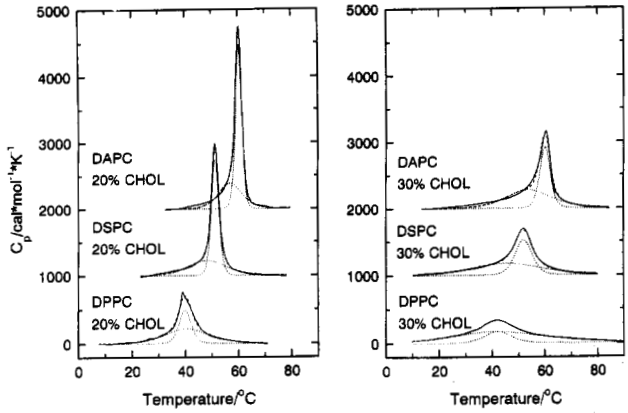


FIGURE 2: DSC thermograms of DPPC, DSPC, and DAPC with 20 and 30 mol % CHOL. The experimental peaks were simulated employing the procedure described in the text using a narrow and a broad-component (see Discussion).

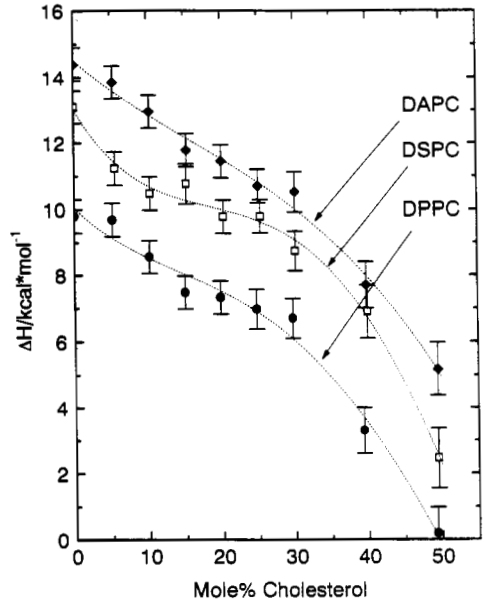


FIGURE 3: Variation of the total transition enthalpy, including the pretransition and the broad component, with CHOL concentration for different PC/CHOL mixtures.

CHOL content, the phase transition is broadened, and the transition enthalpy is descreased and is finally totally abolished. Due to the scan rate of 1 °C/min, the sharp peaks for dispersions with low CHOL content are *slightly* broadened due to the instrumental dead time. At higher CHOL content this effect is negligible and does not affect the shape of the DSC curves. While the general qualitative behavior for all three phospholipids is the same, closer inspection of the DSC scans of DPPC, DSPC, and DAPC/CHOL reveals distinct differences in transition behavior, which are obviously related to the chain length of the phospholipid. Figure 2 shows the DSC peaks of DPPC, DSPC, and DAPC at 20 and 30 mol % CHOL content. Significant differences in the shift of the temperatures for the onset and completion of melting induced by CHOL are evident. For all three lipids the peaks can be decomposed into a sharper and a very broad component. For DPPC/CHOL, the temperature at which melting is complete is shifted to much higher temperatures with increasing CHOL content, in agreement with all previous studies (Ladbrooke et al., 1968; Estep et al., 1978; Mabrey et al., 1978; Vist & Davis, 1990). This effect is not as pronounced in DSPC/CHOL and is almost completely eliminated in DAPC/CHOL. The temperature at the end of the broad peaks is ca. 65–70 °C in all three cases. Only the temperatures at the beginning of the peaks are somewhat different. The area and half-width of the sharp component is clearly dependent on the chain length of the phosphatidylcholine, the DAPC/CHOL mixture displaying the largest area for the sharp component with the smallest half-width. Similar trends are observed at higher CHOL content. Interestingly, the width of the transition at 40 mol % CHOL, being mainly determined by the broad component, is the same for all three systems, extending roughly from below 10 to approximately 90 °C (not shown). Only the heat capacity maxima are at different temperatures, 42 °C for DPPC, 50 °C for DPPC, and 60 °C for DAPC with 40% CHOL, respectively.

The plots of the transition enthalpy $\Delta H$ versus CHOL content in Figure 3 show that the transition of DPPC is completely eliminated at 50 mol %, whereas for 1:1 DAPC/CHOL, a broad transition with an enthalpy of ca. 4 kcal/mol is still visible. This is similar for 1:1 DSPC/CHOL, although the transition is here only half as large.

*Deuterium NMR Spectra of PC/CHOL Mixtures.* The temperature dependence of 2-[12,12-$^2H_2$]DSPC/50 wt % $H_2O$ dispersions in the presence of various CHOL concentrations is shown in Figure 4. Spectra for 2-[6,6-$^2H_2$]DPPC/50 wt

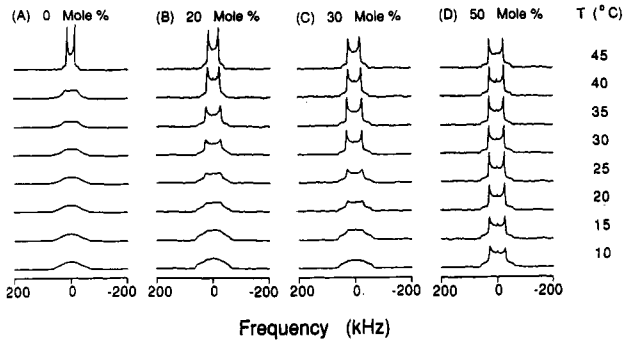


FIGURE 4: Experimental 45.1-MHz $^2H$ NMR spectra of 2-[12,12-$^2H_2$]DSPC/CHOL mixtures in 50 wt %, $^2H$-depleted $H_2O$ at various temperatures and CHOL compositions. Spectra were obtained with a quadrupole echo sequence and plotted on an absolute intensity scale.

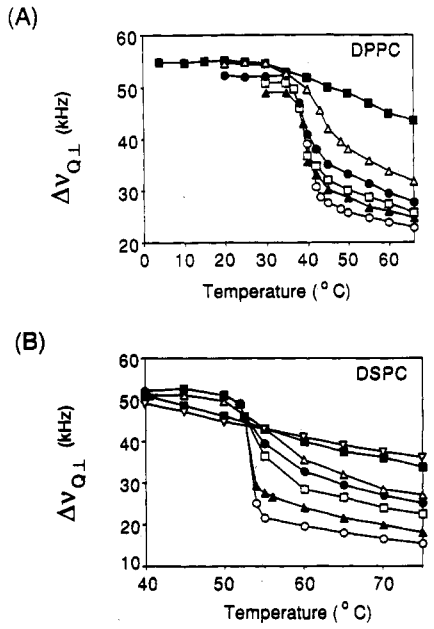


FIGURE 5: Residual quadrupole splitting, $\Delta\nu_{Q\perp}$, as a function of temperature. (A) 2-[6,6-$^2H_2$]DPPC/CHOL: (○) 0 mol % CHOL, (▲) 10 mol % CHOL, (□) 15 mol % CHOL, (●) 20 mol % CHOL, (△) 30 mol % CHOL, (■) 50 mol % CHOL. (B) 2-[12,12-$^2H_2$]DSPC/CHOL: (○) 0 mol % CHOL, (▲) 10 mol % CHOL, (□) 18 mol % CHOL, (●) 24 mol % CHOL, (△) 30 mol % CHOL, (■) 40 mol % CHOL, (▽) 50 mol % CHOL.

% $H_2O$ dispersions and various CHOL concentrations exhibit trends very similar to those of DSPC (not shown). In the absence of CHOL and at low temperatures, a round-top spectrum of ~120-kHz breadth was observed, which transforms to a cone at room temperature. In the $P_{\beta'}$ phase, the spectrum becomes axially symmetric with a parallel splitting of ~116 kHz, and the $P_{\beta'} \rightarrow L_\alpha$ phase transition, the spectrum collapses to a Pake doublet with a splitting $\Delta\nu_{Q\perp}$ of ~30 kHz.

Addition of CHOL alters the spectra in several respects. First, as the CHOL concentration is increased, the narrow Pake doublet spectrum is observed at progressively lower temperatures. However, the size of the splitting $\Delta\nu_{Q\perp}$ is different from that of pure DPPC and increases with increasing [CHOL]. The appearance of the Pake doublet line shape is a clear indication that the lipids are performing fast rotations around the molecular axis. So, with respect to rotational diffusion they are "fluid".

The temperature dependence of $\Delta\nu_{Q\perp}$ for various CHOL concentrations is shown in Figure 5, panels A and B for DPPC and DSPC, respectively. For CHOL concentrations of <20 mol %, the Pake doublet component is observed at temperatures

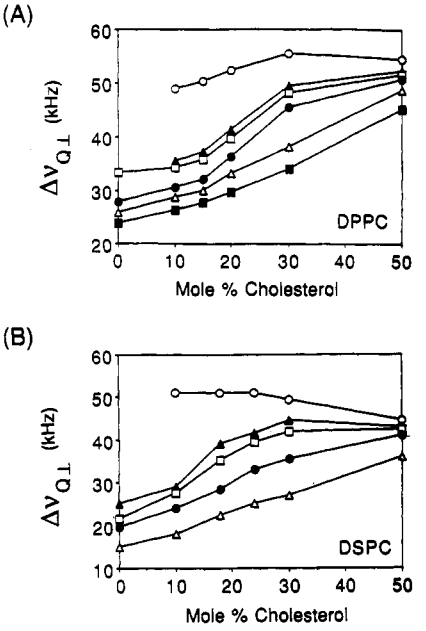


FIGURE 6: Residual quadrupole splitting, $\Delta\nu_{Q\perp}$, as a function of CHOL concentration. (A) 2-[6,6-$^2H_2$]DPPC/CHOL: (○) 30 °C, (▲) 40 °C, (□) 41 °C, (●) 43 °C, (△) 50 °C, (■) 60 °C. (B) 2-[12,12-$^2H_2$]DSPC/CHOL: (○) 50 °C, (▲) 54 °C, (□) 55 °C, (●) 60 °C, (△) 75 °C.

very close to the $T_m$ of the pure lipid and appears as a superposition on top of the gel-phase powder pattern. Also, the values for $\Delta\nu_{Q\perp}$ remain fairly constant but decrease precipitously at the gel → liquid crystal phase transition. However, for high [CHOL] the decrease is linear with no sharp changes.

The concentration dependence of $\Delta\nu_{Q\perp}$ at constant temperature is shown in Figure 6. There is an observable increase in the $\Delta\nu_{Q\perp}$ values as the CHOL concentration is increased. However, this effect is highly dependent on the temperature. In the $L_\alpha$ phase at high temperatures (50–60 °C for DPPC and 60–75 °C for DSPC), the splitting increases almost linearly with [CHOL]. At lower temperatures (but still in the $L_\alpha$ phase) the increase resembles a sigmoidal curve, with the most rapid increases occurring at 20 mol % CHOL. At temperatures below $T_m$ of pure DPPC, yet another behavior is observed. For DPPC at 30 °C, $\Delta\nu_{Q\perp}$ increases up to 30 mol % CHOL and then decreases slightly for higher CHOL concentrations. For DSPC at 50 °C, $\Delta\nu_{Q\perp}$ stays fairly constant for [CHOL] up to 20 mol % and then drops off for higher [CHOL].

*$^{13}C$ NMR Spectra of PC/CHOL Mixtures.* The temperature dependence of 2-[1-$^{13}C$]DSPC/50 wt % $H_2O$ dispersions in the presence of various CHOL concentrations is shown in Figure 7. Spectra of 2-[1-$^{13}C$]DPPC/CHOL dispersions are qualitatively similar in appearance (not shown). The spectral region of interest occurs downfield where the powder pattern from the $^{13}C{=}O$ group is located.

The $^{13}C{=}O$ spectra of the pure PC shown in Figure 7A were previously discussed in detail (Wittebort et al., 1981, 1982). Briefly, the axially asymmetric powder spectrum of the dry powder sample ($\sigma_{11}$ = 260.5 ppm, $\sigma_{22}$ = 140.5 ppm, $\sigma_{33}$ = 117.5 ppm relative to TMS) is characteristic of immobilized phospholipid molecules. Upon dispersion in excess $H_2O$, an axially symmetric spectrum ($\Delta\sigma \simeq 110$ ppm) is observed, indicating the onset of rotational diffusion of the whole phospholipid molecule. The reduced breadth is the result of motional averaging according to the approximation

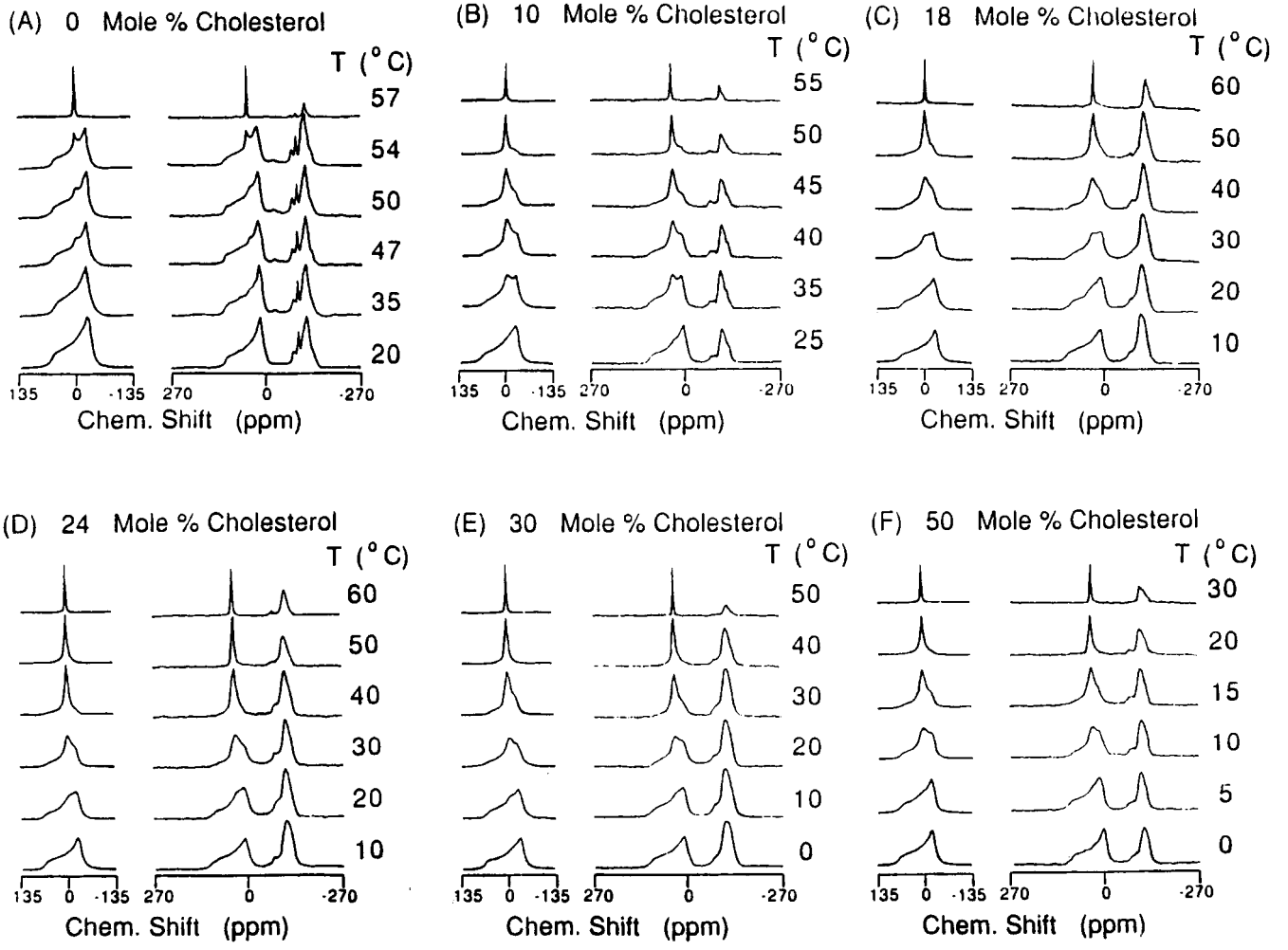


FIGURE 7: Experimental 73.9-MHz $^{13}C$ NMR spectra of 2-[1-$^{13}C$]DSPC/CHOL mixtures in 50 wt % $H_2O$ at various temperatures and CHOL compositions. Spectra in the gel phase were obtained with cross-polarization, followed by a refocusing echo, and are plotted on an absolute intensity scale.

$$\Delta\sigma = \Delta\sigma^{RL}\frac{3\cos^2\theta - 1}{2} \quad (1)$$

where $\Delta\sigma^{RL}$ is the breadth of the rigid lattice powder spectrum. Equation 1 is valid if (i) rotational diffusion is faster than $\gamma H_0\Delta\sigma \simeq 10^4\ s^{-1}$ and (ii) $\Delta\sigma^{RL}$ is axially symmetric. Since the rigid lattice spectrum shows only a slight asymmetry, it can be reasonably represented by an axially symmetric spectrum of breath $\simeq$ 140 ppm. Above the main phase transition ($T_m$ = 41.5 °C for DPPC and 55 °C for DSPC), the spectrum collapses to an isotropiclike line of ~5–10-ppm width, whereas in the $P_{\beta'}$ phase, a temperature-dependent superposition of the spectra was observed. The collapse of the powder pattern to a single line in the $L_\alpha$ phase can be explained by assuming that the *sn*-2 carbonyl of the phospholipid molecule undergoes a conformational change, so that the unique axis of the tensor is tilted to approximately the magic angle ($\theta \simeq 54.74°$).

Before proceeding to the PC/CHOL results, a clarification of the term "$L_\alpha$-like component" is in order. In pure PC and PE bilayers, the sharp component in the $^{13}C{=}O$ spectrum is associated with the appearance of the $L_\alpha$ phase. The appearance of this sharp component is associated with a conformational change of the glycerol backbone so that it resembles that of the $L_\alpha$ phase lipid molecule. As previously noted, the collapse of the broad $L_\beta$ component to a sharp line can be induced by the addition of CHOL at temperatures well below the main phase transition temperature (Blume & Griffin, 1982).

Addition of cholesterol (Figure 7B–F) enhances the population of the $L_\alpha$-like component in the gel phase. For example, for DSPC at 45 °C and 10 mol % CHOL a large fraction of the $L_\alpha$-like component is evident, whereas it is a very minor component in the pure PC spectrum at 47 °C. Another feature of these spectra is the increased line width of the $L_\alpha$-like component as the CHOL content is increased. This is due to increases in the rate of exchange between the two populations ($L_{\beta'}$ and $L_\alpha$-like components) and will be discussed in further detail in the next section.

These spectra have been successfully simulated by a model which assumes exchange between two components corresponding to the $L_{\beta'}$ and $L_\alpha$ populations. The broad component was simulated by assuming a certain angle $\theta$ between the unique axis of the $^{13}C$ tensor and the molecular axis, coupled with fast axial diffusion of the lipid molecule. The narrow component was simulated by assuming fast diffusion and an angle of 54.44° between the molecular axis and the unique axis of the tensor. Thus, the two main variable parameters in the simulations were the relative population of the $L_\alpha$ component, $f_{L\alpha}$, and the exchange rate, $k_{ex}$, between the two components. Although the angle $\theta$ was also varied to better fit the $L_{\beta'}$ component, changes in $\theta$ result in cosmetic changes in the line shape and do not significantly affect $f_{L\alpha}$ or $k_{ex}$. The computer program used for these simulations has been previously described (Wittebort et al., 1987), and the parameters employed to fit the experimental spectra are listed in Tables I and II.

Table I: Parameters Employed in the Computer Simulations of the *sn*-2 $^{13}C{=}O$ Spectra for 2-[1-$^{13}$C]DPPC/CHOL Mixtures

| | mol % CHOL | $T$ (°C) | $f_{L\alpha}$ | $\theta$ | $k_{ex}$ ($s^{-1}$) |
|---|---|---|---|---|---|
| (a) | 0 | 23 | 0.0 | 26 | -- |
| | | 24 | 0.0 | 26 | -- |
| | | 27 | 0.03 | 27 | 9 |
| | | 30 | 0.05 | 28 | 16 |
| | | 33 | 0.13 | 28 | 45 |
| | | 37 | 0.40 | 32 | 200 |
| | | 39 | 0.50 | 32 | 150 |
| | | 42 | 1.00 | 54.74 | -- |
| (b) | 10 | 0 | 0.0 | 29 | -- |
| | | 10 | 0.04 | 31 | 33 |
| | | 15 | 0.10 | 31 | 89 |
| | | 20 | 0.25 | 31 | 267 |
| | | 25 | 0.28 | 33 | 233 |
| | | 30 | 0.40 | 35 | 400 |
| | | 35 | 0.55 | 36 | 367 |
| | | 40 | 1.00 | 54.74 | -- |
| (c) | 15 | 0 | 0.02 | 29 | 20 |
| | | 5 | 0.05 | 30 | 53 |
| | | 10 | 0.10 | 31 | 111 |
| | | 13 | 0.18 | 32 | 176 |
| | | 16 | 0.22 | 32 | 226 |
| | | 19 | 0.35 | 33 | 323 |
| | | 22 | 0.37 | 33 | 352 |
| | | 24 | 0.44 | 35 | 314 |
| | | 26 | 0.45 | 36 | 327 |
| | | 28 | 0.53 | 40 | 226 |
| | | 30 | 0.57 | 40 | 265 |
| | | 32.5 | 0.64 | 40 | 267 |
| | | 35.5 | 0.74 | 40 | 285 |
| | | 40 | 1.00 | 54.74 | -- |
| (d) | 20 | -10 | 0.02 | 29 | 20 |
| | | 0 | 0.04 | 33 | 20 |
| | | 5 | 0.10 | 33 | 111 |
| | | 10 | 0.22 | 33 | 282 |
| | | 15 | 0.33 | 34 | 400 |
| | | 20 | 0.55 | 40 | -- |
| | | 30 | 1.00 | 54.74 | -- |
| | | 40 | 1.00 | 54.74 | -- |
| (e) | 30 | -10 | 0.0 | 33 | -- |
| | | -5 | 0.09 | 33 | 98 |
| | | 0 | 0.28 | 33 | 389 |
| | | 5 | 0.40 | 35 | 533 |
| | | 10 | 0.50 | 40 | 500 |
| | | 20 | 0.80 | 40 | 2000 |
| | | 30 | 1.00 | 54.74 | -- |
| (f) | 50 | -18 | 0.0 | 33 | 250 |
| | | -10 | 0.20 | 34 | 267 |
| | | -5 | 0.25 | 35 | 573 |
| | | 0 | 0.45 | 35 | 663 |
| | | 5 | 0.57 | 40 | 1500 |
| | | 10 | 0.75 | 40 | -- |
| | | 20 | 1.00 | 54.74 | -- |

Table II: Parameters Employed in the Computer Simulations of the *sn*-2 $^{13}C{=}O$ Spectra for 2-[1-$^{13}$C]DSPC/CHOL Mixtures

| | mol % CHOL | $T$ (°C) | $f_{L\alpha}$ | $\theta$ | $k_{ex}$ ($s^{-1}$) |
|---|---|---|---|---|---|
| (a) | 0 | 42 | 0.0 | 27 | -- |
| | | 48 | 0.03 | 27 | 16 |
| | | 50 | 0.05 | 35 | 16 |
| | | 54 | 0.50 | 35 | 28 |
| | | 57 | 1.00 | 54.74 | -- |
| (b) | 10 | 0 | 0.0 | 29 | 33 |
| | | 20 | 0.04 | 31 | 33 |
| | | 25 | 0.04 | 31 | 78 |
| | | 30 | 0.10 | 31 | 132 |
| | | 35 | 0.18 | 32 | 200 |
| | | 40 | 0.33 | 32 | 226 |
| | | 45 | 0.43 | 35 | 375 |
| | | 50 | 0.60 | 40 | -- |
| | | 55 | 1.00 | 75.74 | -- |
| (c) | 18 | 0 | 0.0 | 29 | -- |
| | | 10 | 0.0 | 31 | -- |
| | | 15 | 0.04 | 33 | 38 |
| | | 20 | 0.06 | 33 | 58 |
| | | 30 | 0.15 | 33 | 159 |
| | | 35 | 0.25 | 33 | 267 |
| | | 40 | 0.35 | 35 | 404 |
| | | 45 | 0.47 | 36 | 355 |
| | | 50 | 0.55 | 37 | 367 |
| | | 55 | 0.60 | 37 | 300 |
| | | 60 | 1.00 | 54.74 | -- |
| (d) | 24 | 0 | 0.0 | 31 | -- |
| | | 10 | 0.0 | 33 | -- |
| | | 14 | 0.04 | 33 | 38 |
| | | 20 | 0.15 | 34 | 159 |
| | | 25 | 0.25 | 34 | 267 |
| | | 30 | 0.30 | 35 | 343 |
| | | 35 | 0.45 | 35 | 491 |
| | | 40 | 0.55 | 40 | 489 |
| | | 50 | 0.80 | 40 | 1200 |
| | | 60 | 1.00 | 54.74 | -- |
| (e) | 30 | 0 | 0.04 | 31 | 33 |
| | | 10 | 0.08 | 33 | 70 |
| | | 15 | 0.19 | 33 | 188 |
| | | 20 | 0.25 | 33 | 267 |
| | | 25 | 0.35 | 35 | 377 |
| | | 30 | 0.45 | 36 | 491 |
| | | 35 | 0.55 | 40 | 489 |
| | | 40 | 0.65 | 40 | 557 |
| | | 50 | 1.00 | 54.74 | -- |
| | | 60 | 1.00 | 54.74 | -- |
| (f) | 50 | 0 | 0.0 | 32 | -- |
| | | 5 | 0.05 | 33 | 47 |
| | | 10 | 0.25 | 33 | 300 |
| | | 15 | 0.40 | 35 | 467 |
| | | 20 | 0.75 | 40 | 1200 |
| | | 30 | 1.00 | 54.74 | -- |

Figure 8 shows the change in the fraction of the $L_\alpha$-like component, $f_{L\alpha}$, with temperature at various constant [CHOL] values. The temperature at which the spectrum showed only an isotropic $^{13}C$ NMR spectrum ($f_{L\alpha} = 1$), was obtained by extrapolation of the curves. Extrapolation to the other extreme where $f_{L\alpha} = 0$ provides the temperture at which a single-component $L_\beta$ or $L_{\beta'}$-like spectrum is observed. These temperatures are important in delineating the phase diagram for PC/CHOL mixtures. Figure 9 shows the variation of $f_{L\alpha}$ with CHOL concentration at various constant temperatures for DPPC and DSPC. Again, these curves can be extrapolated to those CHOL concentrations where $f_{L\alpha} = 0$ and $f_{L\alpha} = 1$.

The variation of the exchange rate, $k_{ex}$, with temperature and CHOL concentration is shown in Figures 10 and 11. As noted above, the $^{13}C$ spectra exhibit exchange broadening between the $L_\beta$ and $L_\alpha$-like components at high [CHOL] and temperatures. This is reflected by an increase in the $k_{ex}$ values used in the simulations.

*PC/CHOL Temperature Composition Diagrams.* Temperature/composition diagrams were constructed from the $^2H$ and $^{13}C$ NMR spectra for DPPC and DSPC in the presence of cholesterol. These results, which are qualitatively very similar, are shown in Figures 12 and 13. At low temperatures, the phospholipid exists in the $L_{\beta'}$ phase. The boundary for this phase was obtained from the $^{13}C$ NMR results by extrapolation of the temperature and composition curves from Figures 8 and 9 to the $f_{L\alpha} = 0$ points. The boundary between the gel and liquid crystalline phases was obtained from examination of the $^2H$ NMR results. For CHOL concentrations of <30 mol %, the $^2H$ splitting $\Delta\nu_{Q\perp}$ shows a discontinuity on passing through the gel → liquid crystal transition. Thus, the phase boundary can be delineated by obtaining the midpoints of this transition from Figure 5. For low CHOL concentrations up to 5 mol %, DSC scans reveal that the $P_{\beta'}$ phase is retained (see Figure 1). This is noted on the phase diagrams in Figures 12 and 13 but not confirmed by NMR data. Besides the $L_{\beta'}$ and $P_{\beta'}$ regions, $^{13}C$ NMR revealed two additional regions which we have labeled $LG_I$ and $LG_{II}$ in the phase diagram and which correspond to disordered gel-phase phospholipid at high [CHOL]. The boundary between $LG_I$ and $LG_{II}$ was determined from the

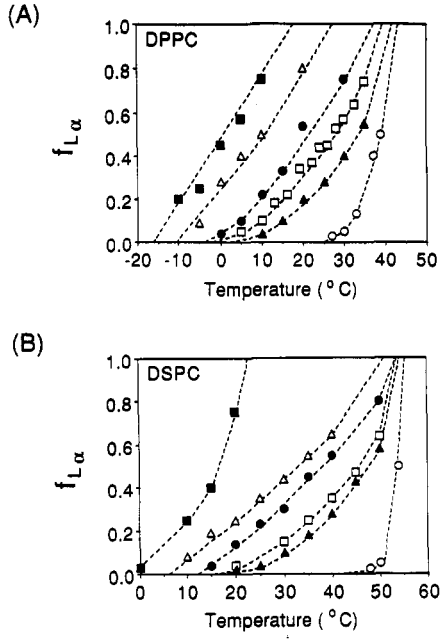


FIGURE 8: Fraction of fluid lipid, $f_{L\alpha}$, as a function of temperature. Results were obtained from computer simulation of the $^{13}C$ NMR spectra in Figure 7 (panel B) and data not shown (panel A). Values for $f_{L\alpha}$ are listed in Tables I and II. (A) 2-[1-$^{13}C$]DPPC/CHOL: (○) 0 mol % CHOL, (▲) 10 mol % CHOL, (□) 15 mol % CHOL, (●) 20 mol % CHOL, (△) 30 mol % CHOL, (■) 50 mol % CHOL. (B) 2-[1-$^{13}C$]DSPC/CHOL: (○) 0 mol % CHOL, (▲) 10 mol % CHOL, (□) 18 mol % CHOL, (●) 24 mol % CHOL, (△) 30 mol % CHOL, (■) 50 mol % CHOL.

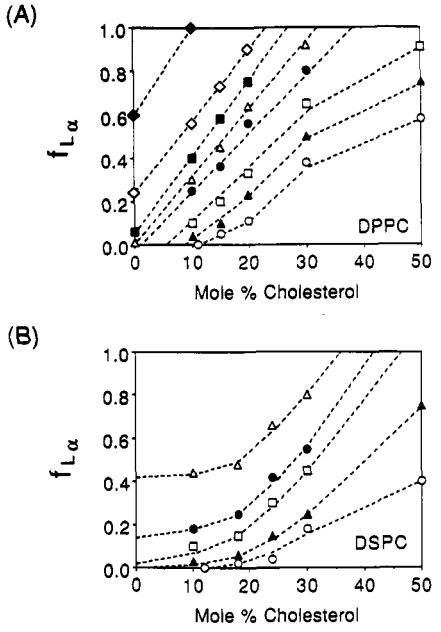


FIGURE 9: Fraction of fluid lipid, $f_{L\alpha}$, as a function of CHOL concentration. Results were obtained from computer simulation of the $^{13}C$ NMR spectra in Figure 7 (panels B–F) and data not shown (panel A). Values for $f_{L\alpha}$ are listed in Tables I and II. (A) 2-[1-$^{13}C$]DPPC/CHOL: (○) 5 °C, (▲) 10 °C, (□) 15 °C, (●) 20 °C, (△) 25 °C, (■) 30 °C, (◇) 35 °C, (◆) 40 °C. (B) 2-[1-$^{13}C$]DSPC/CHOL: (○) 15 °C, (▲) 20 °C, (□) 30 °C, (●) 35 °C, (△) 40 °C.

$^{13}C$ NMR results by extrapolation of the temperature and composition curves to the $f_{L\alpha} = 1$ points. In the region $LG_{II}$ we observe superpositions of gel and fluid-like components by $^{13}C$ NMR. The $^{2}H$ NMR spectra also seem to indicate two different components, although the superposition of sharp Pake pattern and rounded gel-type line shape is not as obvious. The

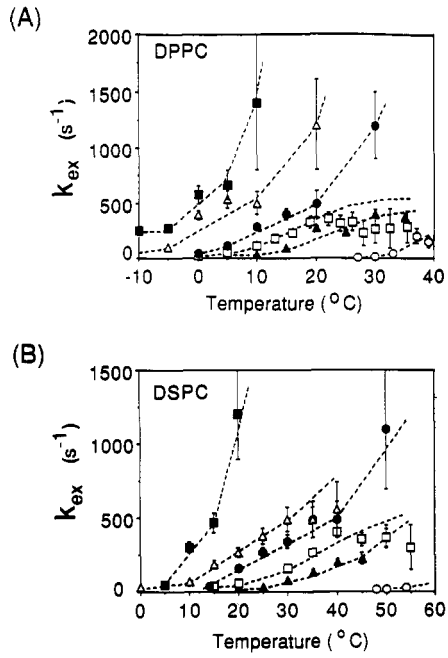


FIGURE 10: Exchange rate constant, $k_{ex}$, between $L_\beta$ and $L_\alpha$-like components as a function of temperature. Results were obtained from computer simulation of the $^{13}C$ NMR spectra in Figure 7 (panel B) and data not shown (panel A). Values for $k_{ex}$ are listed in Tables I and II. (A) 2-[1-$^{13}C$]DPPC/CHOL: (○) 0 mol % CHOL, (▲) 10 mol % CHOL, (□) 15 mol % CHOL, (●) 20 mol % CHOL, (△) 30 mol % CHOL, (■) 50 mol % CHOL. (B) 2-[1-$^{13}C$]DSPC/CHOL: (○) 0 mol % CHOL, (▲) 10 mol % CHOL, (□) 18 mol % CHOL, (●) 24 mol % CHOL, (△) 30 mol % CHOL (■) 50 mol % CHOL.

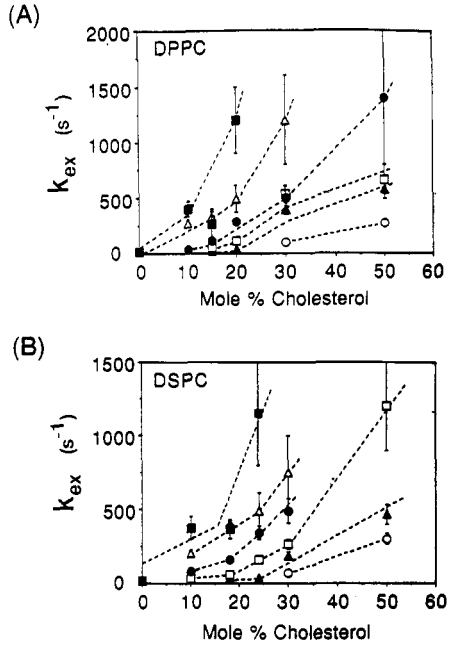


FIGURE 11: Exchange rate constant, $k_{ex}$, between $L_\beta$ and $L_\alpha$-like components as a function of CHOL concentration. Results were obtained from computer simulation of the $^{13}C$ NMR spectra in Figure 7 (panel B–F) and data not shown (panel A). Values for $k_{ex}$ are listed in Tables I and II. (A) 2-[1-$^{13}C$]DPPC/CHOL: (○) −5 °C, (▲) 0 °C, (□) 5 °C, (●) 10 °C, (△) 20 °C, (■) 30 °C. (B) 2-[1-$^{13}C$]DSPC/CHOL: (○) 10 °C, (▲) 15 °C, (□) 20 °C, (●) 30 °C, (△) 40 °C, (■) 50 °C.

significance of these different regions will be discussed in the next section.

## DISCUSSION

*Differential Scanning Calorimetry.* DSC has been one of the most widely used methods for studying lipid/CHOL

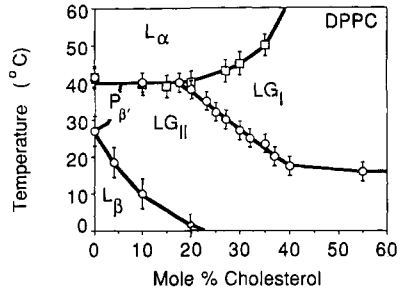


FIGURE 12: Temperature composition diagram for the DPPC/CHOL system. (□) Data points from $^2H$ NMR. (○) Data points from $^{13}C$ NMR.

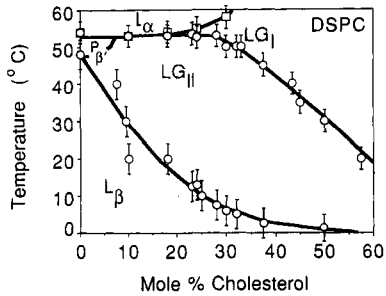


FIGURE 13: Temperature composition diagram for the DSPC/CHOL system. (□) Data points from $^2H$ NMR. (○) Data points from $^{13}C$ NMR.

interactions (Ladbrooke et al., 1968; Estep et al., 1978; Mabrey et al., 1978; Blume, 1980; Davis & Keough, 1983; Vist & Davis, 1990). In a number of lipid/CHOL systems the DSC traces show the appearance of two overlapping peaks of different width, commonly referred to as the sharp and broad components. While these two components are quite obvious in DMPC/CHOL and DPPC/CHOL mixtures, their presence is less evident in other mixtures, although a decomposition into two components was possible for mixed-chain PCs and DSPC/CHOL (Davis & Keough, 1983). As is shown in Figures 1–3, the transition enthalpy does not go to zero in mixtures of DSPC and DAPC with 50 mol % CHOL, as is the case for phospholipids with shorter chain lengths such as DPPC.

The decomposition of the DSC peaks using a two-state transition model with different van't Hoff transition enthalpies is possible in principle. The DSC results for DPPC/CHOL show that even at 30 mol % CHOL the endotherm can be decomposed into two components. This differs from previous results, where the disappearance of the narrow component was described as occurring around 20 mol % CHOL. However, there exist considerable difficulties in establishing a correct interpretation of the DSC results because the transitions are extremely broad, covering a temperature range of almost 90 °C. Only with a DSC instrument with a highly reproducible base line, such as the DASM-1M used in these investigations, is it possible to detect and analyze these broad transitions following subtraction of the base line due to the buffer. Thus, as shown in this study, the broad transition covers a much wider temperature range than previously reported using other DSC instruments. The interpretation of these two components appearing in the DSC traces in terms of a phase diagram, with the phase boundaries being determined by the onset and end temperatures of the two peaks, is ambiguous for the following reason. For the decomposition shown in Figure 2, a simple two-state transition with the cooperativity entering as a variable parameter was used. Certainly, this model is an oversimplification of the real situation, but with this approach the DSC curves can be described as consisting of at least two peaks. Any other more complicated transition model could lead to a single peak of different shape than the two-state model. The onset and end temperatures of the narrow and broad components thus depend on the transition model used for the simulations. As there is no justification for the simple two-state model, only the onset and end temperatures for the total transition might be meaningful. We will discuss these below.

The phospholipid chain length dependence of the CHOL effect can be explained by the difference in molecular length between CHOL and the fatty acyl chain of the phospholipid. If the side chain is fully extended and the OH group on the sterol ring is excluded, CHOL has a length of ~18.4 Å. This can be contrasted with a chain of 16 Cs, which has a length of ~20 Å. The disparity is even greater for longer chain lengths, such as those in DAPC, where the difference in molecular length is 6.5 Å when compared to CHOL. Since CHOL acts as a spacer between phospholipid molecules, this molecular length difference creates a free volume in the middle of the bilayer which is energetically unfavorable. There is low-angle X-ray scattering evidence (McIntosh, 1978) that the ends of the chain probably tilt to maximize the van der Waals interactions. This can also be deduced from changes in the bilayer thickness as determined from monolayer and densitometry experiments (Blume, to be published). Additionally, the chain ends may have a kink to fill the void volume created by the shorter CHOL molecule. Indeed, McIntosh also reported the existence of a broad 4.2-Å reflection and attributed this to the hydrocarbon tails being in a different state from the normal liquid crystalline one. These residual interactions between the hydrocarbon tails are probably responsible for the observation of a broad endothermic transition for high [CHOL] in the longer chain PCs. Recently, Singer and Finegold (1990) reported DSC studies of PC/CHOL mixtures for PCs with different chain lengths ranging from $C_{12}$ to $C_{20}$. Their results are at variance with our and those of previously published work, as they report vanishing DSC peaks at 26.5 mol % CHOL for DPPC, 32.3 mol % for DSPC, and 43.3 mol % for DAPC. In our experiments we still observed a broad transition for all three lipids at higher CHOL content, in agreement with the results of other groups. The percentages reported by Singer and Finegold seem to coincide more closely with those CHOL mole fractions where the narrow component vanishes and the $^{13}C$ spectra show only a sharp line.

The differences in the DSC curves observed for PCs as a function of chain length highlighted the necessity of performing a chain lenth-dependent NMR study of the PC/CHOL system. Examination of just one lipid species, such as DPPC, is insufficient and a variety of PCs must be sampled to determine the overall trends. Hence, the NMR portion of this study consists of a systematic examination of two lipid species, DSPC and DPPC. DAPC was not studied and will remain as a future extension of this work.

*Deuterium NMR Spectra of PC/CHOL Mixtures.* The $^2H$ spectra of DPPC/CHOL and DSPC/CHOL mixtures are similar to those of the PE/CHOL system previously studied (Blume & Griffin, 1982) in that they do not exhibit the dramatic changes associated with the $^{13}C$ spectra. Nonetheless, they are informative and complement the $^{13}C$ results, since the $^2H$ spectra provide information in temperature ranges where the corresponding $^{13}C$ spectra have collapsed to a narrow line. In these studies we employed the discontinuity in $\Delta\nu_{Q\perp}$ to delineate the boundary between the gel and liquid crystalline phases. This was especially useful for high CHOL concentrations where the first-order DSC transition disappears and $^{13}C$ spectrum shows only the sharp line.

The DPPE/CHOL study by Blume and Griffin (1982) revealed that CHOL condenses or orders PE in the $L_\alpha$ phase. In the gel phase the $^2H$ spectra of DPPE are ~120 kHz full width, and addition of CHOL does not result in significantly narrower spectra—i.e., a more disordered phase. However, the sterol does induce rapid axial diffusion which results in an axially symmetric line shape. The PC/CHOL spectra reported here show similar effects. The size of $\Delta\nu_{Q\perp}$ for the Pake doublet increases for increasing [CHOL], indicating increased order for the hydrocarbon chains. Also, the appearance of the Pake doublet at progressively lower temperatures in the gel phase results from the ability of CHOL to induce axial diffusion in the gel phase.

A deficiency in the $^2H$ experiment was highlighted in the investigation by Blume and Griffin. Specifically, the spectra do not exhibit clearly separable components which can be attributed to gel or $L_\alpha$ phase; hence, the interpretation of the results is complicated by the need to deconvolute and dissect multiple effects. These $^2H$ spectra must be interpreted in conjunction with $^{13}C$ measurements; then a successful simulation of the line shapes and echo intensities is possible, as shown previously for DPPE/CHOL mixtures (Blume & Griffin, 1982).

*$^{13}C$ NMR Spectra of PC/CHOL Mixtures.* The dramatic narrowing of the $^{13}C$ NMR spectra of the *sn*-2 carbonyl position has been observed for a variety of phospholipid systems, including pure PC and PE (Wittebort et al., 1981, 1982), DPPE/CHOL mixtures (Blume & Griffin, 1982), and DPPC/DPPE mixtures (Blume et al., 1982). The narrowing is attributed to a conformational change of the *sn*-2 carbonyl, possibly from a change in the glycerol backbone conformation. For DPPC in the $L_{\beta'}$ phase, $\theta$, the orientation of the unique axis of the $^{13}C{=}O$ tensor, ranges from 26° ± 2° at room temperature to 32° ± 2° at high temperatures and CHOL concentration (corresponding values for DSPC are 27° ± 2° and 35° ± 2°, respectively). Thus, for $\Delta\sigma \simeq 0$ and $\theta = 54.74°$, there must be a conformational change of ~30° in the tensor orientation on passing through the gel → liquid crystal phase transition.

Several interesting features can be observed in the $^{13}C$ results. First, the addition of a high amount of CHOL results in the collapse of the broad $L_{\beta'}$ or $L_\beta$-like powder pattern to the sharp $L_\alpha$-like line at temperatures well below the main gel → liquid crystal phase transition tempertaure of the pure lipid. Second, at intermediate CHOL concentrations and lower temperatures we observe two-component spectra, i.e., superpositions of $L_\alpha$-like lines and a gel-type spectrum. At higher CHOL concentrations and/or temperature the $L_\alpha$-like component is broadened such that the spectrum assumes a "triangular" shape. This observation indicates a dynamic equilibrium between the two spectral components with exchange rates in the intermediate exchange regime of the $^{13}C$ NMR experiment. All line shapes could be successfully simulated by varying the exchange rates and the fractions of the two components.

The results of these simulations lead to the following conclusions. First, the fractions of the two components vary with CHOL content and temperature. Second, the angle $\theta$ for the orientation of the unique axis of the $^{13}C{=}O$ tensor for the gel-like component increases with CHOL content. This is different compared to the DPPE/CHOL system, where all spectra could be simulated with the same angle $\theta$ of ~28°. Apparently, the change in $\theta$ on CHOL incorporation into DPPC or DSPC reflects the change in tilt of the hydrocarbon chains going from an $L_{\beta'}$ to an $L_\beta$ phase. The fact that CHOL removes the chain tilt is known from X-ray investigations (McIntosh, 1978). Third, the broadening of the $L_\alpha$-like component also varies with CHOL concentration and temperature. The simulated spectra reflect this trend, since $k_{ex}$ must be increased to obtain satisfactory fits with the experimental data. As shown in Figures 10 and 11, $k_{ex}$ increased with increasing temperature and [CHOL], with the most dramatic increases occurring for CHOL concentrations above 20 mol %.

Since $k_{ex}$ is a measure of the translational diffusion between the two lipid domains, it can be used to estimate the distance separating the two domains, i.e., the gel-like and the "liquid–gelatin" domain. The area of a domain can be roughly estimated from the mean square displacement (Saffman & Delbrück, 1975; Blume & Griffin, 1982) according to the equation

$$x^2 = 4D_T t \qquad (2)$$

where $D_T$ is the diffusion coefficient and $t$ is the exchange lifetime. For a CHOL concentration of 30 mol % with a fluid fraction $f_{L\alpha} = 0.5$, an exchange rate of ~500 $s^{-1}$ was extrapolated for both DPPC and DSPC. This yields an exchange lifetime value of 2.0 ms. Taking a value of $1 \times 10^{-10}$ $cm^2$ $s^{-1}$ for $D_T$ (Rubenstein et al., 1979), this results in a mean square displacement value of $8 \times 10^3$ Å$^2$. This area corresponds to a cluster of ~100 lipid molecules, a result which is similar to that reported for DPPE/CHOL (Blume & Griffin, 1982). However, these estimations have to be viewed with caution. In the fluorescence photobleaching recovery (FPR) experiment the lateral diffusion coefficient $D_T$ is measured over distances of the order of micrometers (Vaz et al., 1982). This is in contrast to experiments with excimer probes, where the distances are of the order of 10 Å. In this case, one measures essentially the exchange between neighboring molecules (Galla et al., 1979; Sassaroli et al., 1990). The $D_T$ values obtained with excimer probes for gel-state DMPC bilayers are at least 2 orders of magnitude higher than those determined by FPR (Sassaroli et al., 1990). Therefore, for long-range diffusion the bilayer behaves more like a solid in the $L_{\beta'}$ and the $P_{\beta'}$ phase, while a relatively high "fluidity" is observed locally. Surely, this also applies to PC/CHOL systems, which complicates the interpretation of the $k_{ex}$ values in terms of domain sizes.

Monte Carlo simulations of PC/CHOL bilayers (Snyder & Freire, 1980; Cruzeiro-Hansson et al., 1989; Ipsen et al., 1989) show that in these systems clustering of "gel-like" and "fluid-like" molecules occurs. The clusters are relatively small in size, the number of molecules in a cluster increasing as the midpoint of the transition is approached. In all cases, the clusters are small, comprising less than 50 molecules (Cruzeiro-Hansson et al., 1989). A further important finding of these calculations is that cholesterol does not seem to be distributed randomly in the plane of the bilayer but tends to be concentrated at domain boundaries. This was previously suggested on the basis of neutron scattering results on DMPC/CHOL mixtures, although an even more organized lateral distribution of cholesterol molecules was suggested (Mortensen et al., 1988). This cholesterol clustering at domain boundaries could also have an effect on the lipid exchange between different domains, since it could act as a diffusion barrier. In any case, the observed exchange rates and estimated domain sizes are consistent with the picture of a cluster organization of the PC/CHOL membrane in the region $LG_{II}$. The temperature dependence of the $k_{ex}$ values does not give a straight line in an Arrhenius plot, indicating that the underlying exchange is not a simple activated process. Cooperative phenomena and/or changes in connectivity of the domains

are probably responsible for this behavior.

*PC/CHOL Temperature Composition Diagram.* Considering the microscopic structure of PC/CHOL bilayers, it seems problematic to discuss the properties determined by $^2H$ and $^{13}C$ NMR in terms of a phase diagram. Nevertheless, we observe changes in lipid mobility and conformation as a function of temperature and CHOL concentration. A temperature/composition diagram can be constructed with different regions in which the PC molecules show different mobility and conformation. We have labeled these different regions $L_{\beta'}$, ($L_\beta$), $L_\alpha$, $LG_I$, and $LG_{II}$, depending on the NMR spectral parameters. These "phase diagrams" look similar for DPPC/CHOL and DSPC/CHOL. However, there are subtle differences. The $P_{\beta'}$ region for DSPC is slightly smaller than that for DPPC as the pretransition and the main transition are closer together. The position of the line separating region $LG_{II}$ from $LG_I$ is dependent on the chain length of the PC. For DSPC this line is shifted toward higher CHOL concentrations compared to DPPC. This agrees with previous experiments on DMPC/CHOL (Wittebort et al., 1982), where for all temperatures above 0 °C only a sharp $L_\alpha$-like line was observed when the CHOL content exceeded 25 mol %. In addition, a headgroup influence on the position of this line appears to exist, as in the DPPE/CHOL system it is intermediate between DPPC/CHOL and DSPC/CHOL (Blume & Griffin, 1982). The $LG_{II}$ region is clearly characterized by two-component $^{13}C$ and probably also $^2H$ NMR spectra, while in the $LG_I$ region only one-component spectra are observed. The temperatures delineating the boundary between the $L_\beta$ and $LG_{II}$ region were determined from the $^{13}C$ NMR spectra. The appearance of the narrow component in the $^{13}C$ NMR line shapes coincides roughly with the beginning of the broad DSC peak, as shown in Figures 1 and 2. Thus, the $^{13}C$ NMR spectra are very sensitive to the beginning of "melting", a phenomenon which has been observed before for other systems (Blume et al., 1982; Blume & Griffin, 1982). The onset and end tempertures for the narrower components of the DSC peaks for the DPPC and DSPC systems follow more or less the boundaries between the $LG_{II}$ and $LG_I$ and the $LG_I$ and $L_\alpha$ regions, respectively. However, the onset temperatures for the broad components are always lower than the boundary line between $LG_{II}$ and $LG_I$ as determined by NMR (see Figure 2).

With the assumption that the $LG_{II}$ region is indeed a two-phase region with equilibrium between $L_{\beta'}$($L_\beta$) and a "liquid–gel" component, we can compare our "phase diagram" with those reported earlier using other methods. Only certain sections of our phase diagrams agree with previous studies (Recktenwald et al., 1979; Lentz et al., 1980; Mortensen et al., 1988; Vist & Davis, 1989). Our results indicate a horizontal line between the gel and $L_\alpha$ phases for CHOL concentrations <20 mol %. For higher [CHOL] our $^2H$ NMR results delineate an upward curve in this phase boundary, as was observed in the earlier studies. As for the rest of the phase diagram, there are distinct differences between our results and those listed above.

One major difference between the previously published results and this study lies in the delineation of the $LG_I$ and $LG_{II}$ phase boundary. Most published phase diagrams denote this boundary by a *vertical* line at a concentration of 20 mol % CHOL [for example, see Shimshick and McConnell (1973b), Recktenwald et al. (1973), Gershfeld (1978), Lentz et al. (1980), Rand et al. (1980), and Mortensen et al. (1988)]. This is clearly not the case as determined from the $^{13}C$ NMR spectra in this study. If this boundary were vertical, then the sharp $L_\alpha$-like line would be the sole component of the $^{13}C$ spectrum for CHOL concentrations >20 mol % at any given temperature in the gel phase, and this would be reflected by a discontinuity in the curves shown for Figure 9. In particular, one would expect that $f_{L\alpha}$ would approach 1.0 at the discontinuity and this should occur at 20 mol %. Instead, the $f_{L\alpha}$ versus [CHOL] isotherms appear sigmoidal or linear, and there is not discernible discontinuity. Hence, the $LG_I/LG_{II}$ phase boundary in Figures 12 and 13 are nonlinear and far from vertical as previously reported. The recent publication of Vist and Davis (1990) considered a limited temperature/concentration range in this region of the phase diagram and, as mentioned in their paper, the errors in their measurements for this particular region were large. Thus, they were not able to elucidate the position of the $LG_I/LG_{II}$ boundary with precision.

Recent theoretical work on the DPPC/CHOL system by Ipsen et al. (1989) using a mean field approximation shows a phase diagram in which the line separating the two-phase from the one-phase regions is not vertical but slopes toward higher CHOL concentrations. This is exactly what we observe by $^{13}C$ NMR. However, these mean field calculations were performed by neglecting effects due to inhomogeneous lateral distributions of CHOL and domain formation. As shown by the same group of workers (Cruzeiro-Hansson et al., 1989), these phenomena do indeed occur. According to Ipsen et al., this would not affect the general form of the phase diagram, but of course lateral inhomogeneity and domain formation would affect our $^{13}C$ spectra, so that the agreement between our results and the theoretical calculations has to be viewed with caution. Nevertheless, the regions we label $LG_I$ and $LG_{II}$ do correspond to the regions denoted *1* o and so-*1* o, respectively, by Ipsen et al. (1987, 1989).

Recently published experimental results (Vist & Davis, 1990) and the theoretical work mentioned above (Ipsen et al., 1987, 1989) report an additional two-phase region between $L_\alpha$ phase and the $LG_I$ region with a critical point at higher temperature. In the experiments of Vist and Davis the phase boundaries were determined from the end of melting of the broad component in the DSC peaks and from the sharpening of the $^2H$ NMR spectra. Our temperatures for the end of melting do not agree with those reported by Vist and Davis but are considerably higher, even after correction for the effect of perdeuteration of the chains. Specifically, the end temperature for the broad component in the DPPC/CHOL mixtures is ca. 55 °C at 15 mol %, 60 °C at 20 mol %, and more than 80 °C at 30 mol % CHOL (see Figure 2). As the broad DSC peak is probably caused by multiple effects, i.e., noncooperative changes of the heat capacity and/or broad second-order transition, the interpretation of the end temperatures of the broad DSC peaks is difficult. In addition, measurements of the specific volume of DPPC/CHOL systems (Melchior et al., 1980) show that the differences in specific volume between DPPC/CHOL bilayers of low and high CHOL content are very small at temperatures above 40 °C, so that a larger difference in the enthalpies which gives rise to an enthalpic effect in the DSC experiment is unexpected. The line separating the two-phase region from the "liquid–gelatin" phase cannot be determined from our NMR experiments, since all spectra indicate fast exchange. (A notable sharpening of the $^2H$ NMR resonances, as reported by Vist and Davis, could not be observed.) If this detail is excluded, then the $^{13}C$ NMR "phase diagram" agrees well with the theoretical phase diagram reported by Ipsen et al. (1989).

## CONCLUSIONS

This calorimetric and NMR study of PC/CHOL mixtures revealed rather complex phase behavior for this simple, binary

system. DSC of these mixtures showed a gradual disappearance of the first-order gel → liquid crystalline transition as the CHOL content increased, indicating a loss of cooperativity at high CHOL concentrations. The CHOL content at which the sharp component in the DSC curve vanishes depends on the lipid chain length increasing in the order DPPC, DSPC, and DAPC. The NMR spectra (both $^2H$ and $^{13}C$) continued to show spectroscopic changes, even after all cooperativity was lost. Analysis of the NMR spectra resulted in characterization of a new phase which we have termed "liquid–gel". This "liquid–gel" phase shows increased fluidity compared to the $L_{\beta'}$ or $L_\beta$ phase of the pure phospholipid bilayer. Specifically, this "phase" is characterized by an almost all-*trans* conformation of the lipid acyl chains and fast axial diffusion of the whole molecule. In the two-phase region between the $L_{\beta'}(L_\beta)$ and the "liquid–gel" phase we observed two-component $^{13}C$ spectra, which indicate fast exchange between domains of different state and composition. Estimations on the basis of reported values of the lateral diffusion coefficients lead to the conclusion that these domains are small, in agreement with electron and neutron scattering results and theoretical calculations. In addition, it seems probable that a heterogeneous distribution of CHOL in these domains exists. Partial "phase diagrams" were presented for DPPC/CHOL and DSPC/CHOL mixtures. These "phase diagrams" agree qualitatively with some previous studies and show consistent trends between lipid species of differing chain lengths.

## ACKNOWLEDGMENT

The authors would like to thank J. H. Davis for communicating his results to us prior to publication and M. J. Ruocco, D. J. Siminovitch, J. B. Speyer, and R. T. Weber for fruitful discussions during the course of this work.

## REFERENCES

Blume, A. (1980) *Biochemistry 19*, 4908–4913.
Blume, A. (1983) *Biochemistry 22*, 5436–5442.
Blume, A., & Griffin, R. G. (1982) *Biochemistry 24*, 6230–6242.
Blume, A., Wittebort, J. R., Das Gupta, S. K., & Griffin, R. G. (1982) *Biochemistry 21*, 6243–6253.
Brown, M. F., & Seelig, J. (1978) *Biochemistry 17*, 381–384.
Calhoun, W. I., & Shipley, G. G. (1979) *Biochemistry 18*, 1717–1722.
Copeland, B. R., & McConnell, H. M. (1980) *Biochim. Biophys. Acta 599*, 95–109.
Cruzeiro-Hansson, L., Ipsen, J. H., & Mouritsen, O. G. (1989) *Biochim. Biophys. Acta 979*, 166–176.
Cullis, P. R., Hope, M. I., De Kruijff, B., Verkleif, A. J., & Tilcock, C. P. S. (1985) in *Phospholipid and Cellular Regulation* (Kuo, J. F., Ed.) Vol. 1, pp 1–59, CRC Press, Boca Raton, FL.
Das Gupta, S. K., Rice, D. M., & Griffin, R. G. (1982) *J. Lipid Res. 23*, 197–200.
Davis, J. H., Jeffrey, K. R., Bloom, M., Valic, M. I., & Higgs, T. P. (1976) *Chem. Phys. Lett. 42*, 390–394.
Davis, P. J., & Keough, K. M. W. (1983) *Biochemistry 22*, 6334–6340.
Demel, R. A., & De Kruijff, B. (1976) *Biochim. Biophys. Acta 457*, 109–132.
Estep, T. N., Mountcastle, D. B., Biltonen, R. I., & Thompson, T. E. (1978) *Biochemistry 17*, 1984–1989.
Galla, H. J., Hartmann, W., Theilen, U., & Sackmann, E. (1989) *J. Membr. Biol. 48*, 215–236.
Gally, H. U., Seelig, A., & Seelig, J. (1976) *Hoppe-Seyler's Z. Physiol. Chem. 357*, 1447–1450.
Gershfeld, N. L. (1978) *Biophys. J. 22*, 469–488.
Genz, A., Holzwarth, J. F., & Tsong, T.-Y. (1986) *Biophys. J. 50*, 1043–1051.
Griffin, R. G. (1976) *J. Am. Chem. Soc. 98*, 851–853.
Gupta, C. M., Radakrishan, P., & Khorana, H. G. (1977) *Proc. Natl. Acad. Sci. U.S.A. 74*, 4315–4319.
Haberkorn, R. A., Griffin, R. G., Meadows, M. D., & Oldfield, E. (1977) *J. Am. Chem. Soc. 99*, 7353–7355.
Hague, J. L., & Bright, H. A. (1941) *J. Res. Natl. Bur. Stand. 26*, 405.
Hui, S. W., & He, N. B. (1983) *Biochemistry 22*, 1159–1164.
Huang, C. (1977) *Lipids 12*, 348–356.
Ipsen, J. H., Karlström, G., Mouritsen, O. G., & Zuckermann, M. J. (1987) *Biochim. Biophys. Acta 905*, 162–172.
Ipsen, J. H., Mouritsen, O. G., & Zuckermann, M. J. (1989) *Biophys. J. 56*, 661–667.
Jacobs, R., & Oldfield, E. (1979) *Biochemistry 18*, 3280–3285.
Ladbrooke, B. D., Williams, R. M., & Chapman, D. (1968) *Biochim. Biophys. Acta 150*, 333–340.
Lentz, B. R., Barrow, D. A., & Heochli, M. (1980) *Biochemistry 19*, 1943–1954.
Mabrey, S., Mateo, P. L., & Sturtevant, J. M. (1978) *Biochemistry 17*, 2464–2468.
McIntosh, T. J. (1978) *Biochim. Biophys. Acta 513*, 43–58.
Melchior, D. L. (1982) *Curr. Top. Membr. Transp. 17*, 263–316.
Melchior, D. L., Scavitto, F. J., & Steim, J. M. (1980) *Biochemistry 19*, 4828–4834.
Mortensen, K., Pfeiffer, W., Sackmann, E., & Knoll, W. (1988) *Biochim. Biophys. Acta 945*, 221–245.
Pines, A., Gibby, M. G., & Waugh, J. S. (1973) *J. Chem. Phys. 59*, 569–590.
Rand, R. P., Parsegian, V. A., Henry, J. A. C., Lis, L. J., & McAlister, M. (1980) *Can. J. Biochem. 58*, 959–967.
Recktenwald, D. J., & McConnell, H. M. (1981) *Biochemistry 20*, 4505–4510.
Rubenstein, J. L. R., Smith, B. A., & McConnell, H. M. (1979) *Proc. Natl. Acad. Sci. U.S.A. 76*, 15–18.
Saffmann, P. G., & Delbrück, M. (1975) *Proc. Natl. Acad. Sci. U.S.A. 72*, 3111–3113.
Sassaroli, M., Vauhkonen, M., Perry, D., & Eisinger, J. (1990) *Biophys. J. 57*, 281–290.
Shah, D. O., & Schulmann, J. H. (1967) *J. Lipid Res. 8*, 215–226.
Shimshick, E. J., & McConnell, H. M. (1973a) *Biochemistry 12*, 2351–2360.
Shimshick, E. J. & McConnell, H. M. (1973b) *Biochem. Biophys. Res. Commun. 53*, 446–451.
Singer, M. A. & Finegold, L. (1990) *Biophys. J. 57*, 153–156.
Snyder, B., & Freire, E. (1980) *Proc. Natl. Acad. Sci. U.S.A. 77*, 4055–4059.
Stockton, G. W. & Smith, I. C. P. (1976) *Chem. Phys. Lipids 17*, 251–263.
Vaz, W. L. C., Derzko, Z. I., & Jacobson, K. A. (1982) *Cell Surf. Rev. 8*, 83–136.
Vist, M., & Davis, J. H. (1990) *Biochemistry 29*, 451–464.
Wittebort, R. J., Schmidt, C. F., & Griffin, R. G. (1981) *Biochemistry 20*, 4223–4228.
Wittebort, R. J., Blume, A., Huang, T.-H., Das Gupta, S. K., & Griffin, R. G. (1982) *Biochemistry 21*, 3487–3502.
Wittebort, R. J., Olejniczak, E. T., & Griffin, R. G. (1987) *J. Chem. Phys. 86*, 5411–5420.
Yeagle, P. (1985) *Biochim. Biophys. Acta 822*, 267–287.